PAPER

Zirconia/phenylsiloxane nano-composite for LED encapsulation with high and stable light extraction efficiency†

Ying Lu,‡[ab] Zhihang Zhao,‡[a] Xianpeng Fan,[a] Xinyu Cao, [iD] *[a] Mingtan Hai,[b] Zhou Yang,*[b] Kun Zheng, [iD] [a] Jiaxin Lu,[a] Jingnan Zhang, [iD] [a] Yongmei Ma, [iD] *[a] Rongben Zhang[a] and Shibi Fang[a]

To obtain a rapid processible LED encapsulant that leads to high and stable light extraction efficiency (LEE), UV curable ZrO_2/phenyl-siloxane nano-composite (ZSC) double-layer encapsulants were prepared and optimized. The highly crystalline ZrO_2 nanoparticles with a diameter of ~14 nm were synthesized through a modified hydrothermal method at mild conditions, and a UV curable methacryl-diphenyl-polysiloxane (MDPS) with a refractive index (RI) of 1.54 (at 633 nm) was synthesized from self-condensation of diphenylsilanediol and an end-capping reaction. High refractive indexes (RIs) from 1.54–1.61 have been obtained for ZSC composites by adding 0–20 wt% ZrO_2. Before and after sulfur vapor erosion, the double-layer encapsulated sample (M-10/M) showed 11.2% and 64.8% higher LEE respectively than that of Dow Corning OE-7662. Meanwhile, the variation of LED light color temperature (T_c) was less than 1%. The effect of the ZrO_2 nanoparticle content on LEE of double-layer and single-layer encapsulation were compared and discussed based on Fresnel loss and Rayleigh scattering theories. The double-layered UV curing processing took only 1/6 of the time needed for common thermal curing.

1 Introduction

Light-emitting diodes (LEDs) have been widely accepted as light sources in various circumstances owing to their low power consumption and long lifetime. The encapsulation materials that directly contact the blue-chip provide close protection to the package, and also seriously affect its output efficiency and stability.[1] Silicone-based materials have become the most studied encapsulants for LEDs because of their high transparency and resistance to ultraviolet (UV) radiation and heat.[2] Nevertheless, silicone materials are classical with a refractive index (RI) of ~1.4–1.5, which is much lower than that of the LED substrate (~2.6 for GaN or 3.5 for GaP). The mismatch of RI can dramatically reduce the light extraction efficiency (LEE) due to light loss at the interface. On the other hand, because of the extreme flexibility of silicone chains, their gas or vapor permeation is quite high and is harmful to the inner metal components and leads to quick decline or even extinction of the light.

A lot of efforts have been made to increase the RI of silicone materials[3–6] and their gas barrier properties[7–11] to enhance the light extraction efficiency (LEE) value and stability.

The RI of material is contributed by the sum of each chemical unit and composite, so there are generally two ways to increase the RI of silicone materials. One is to introduce organic groups with high polarizability and small molecular volume to the molecular chain or substituents by a chemical bond, such as halogen atoms, sulfur atoms, and π-conjugated groups. In considering thermal stability and cost, phenyl siloxanes[12–18] are the most commonly used. However, with the highest phenyl substitution, the siloxanes may still subject to a RI ceiling of ~1.6.[19–22]

The other way to increase the RI of siloxane is by introducing inorganic nanoparticles with high RI, such as ZrO_2, TiO_2, and ZnO into the matrix. The RI of the composite can be varied in a wide range according to the method of preparation and nanoparticle content. To maintain the transparency of the composite, the particle size, fraction, and dispersion in the matrix are critical. Studies have shown that when the size of the inorganic particles is less than one-tenth of the wavelength of visible light, especially 20 nm, the light scattering of the nanocomposite can be greatly reduced.[13,23]

The copolymerization of Si and A (Zr,[2,24–26] Ti,[27–29] Zn,[30] *etc.*) base precursors by the sol–gel process can lead to high transparent hybrid material, in which the hybrid nano-domains are uniformly dispersed and form Si–O–A bond with silicone.[2] In some stepwise sol–gel methods, ZrO_2,[23,31] TiO_2 (ref. 22 and 32)

[a]*Key Laboratory of Green Printing, Institute of Chemistry, Chinese Academy of Sciences, Beijing 100190, China. E-mail: xinyucao@iccas.ac.cn; yangz@ust.edu.cn; maym@iccas.ac.cn*

[b]*Department of Materials Physics and Chemistry, School of Materials Science and Engineering, University of Science and Technology Beijing, Beijing, 100083, China*

† Electronic supplementary information (ESI) available. See DOI: 10.1039/d1ra02230j

‡ These authors contributed equally to this work.

particles are formed *in situ* and then further composite with siloxanes. The RI was reportedly reached 1.59 (ref. 24) to 1.60.[22]

The introduction of crystalline ZrO_2,[1,33–43] TiO_2 (ref. 44–49) nanoparticles into siloxane are more effective to increase the RI because the RI of the nanoparticle increases dramatically with crystallinity. ZrO_2 has excellent optical properties, such as Abbe number and transparency on a broad spectral range,[50] as well as chemical inertness and thermal stability. ZrO_2/siloxane nanocomposites with RIs of 1.7–1.9 were reported when the mass fraction of the nanoparticles raised to 50% (ref. 1 and 38) to 80%.[50] It is well aware that the nano-particles tend to aggregate in high loading. The optical transparency and mechanical property of the material could be much compromised at such high ZrO_2 content.[23,50] A few reports did demonstrate 10–13% LEE enhancement by using ZrO_2/epoxy or siloxane composite encapsulation with ZrO_2 loading of ∼50 wt%. However, the LEE stabilities were reportedly decreased compare with the matrixes.[1,41,42] It could be caused by a large amount of un-condensed Zr–OH in the system.

Here, we report a UV curable transparent ZrO_2/siloxane nano-composite (ZSC) with an RI of 1.55–1.61 at 5–20 wt% ZrO_2 loading. The ∼14 nm ZrO_2 was highly crystalline and the surface Zr–OHs were sealed by a mono-OH silane coupling agent. The high RI silicone resin was a methacrylate-end-capped polydiphenylsiloxane (MDPS resin) with an RI of 1.54. Furthermore, double-layer LED encapsulation was designed and optimized based on the Fresnel loss theory, and experimental data. The double-layered encapsulant demonstrated an effective and efficient utilization of such the composite that leads to 11% and 65% higher LEE and anti-sulfuric corrosion respectively compared to commercial high RI product Dow Corning OE-7662, and the LEE is also higher than the ZSC single-layer encapsulation. Meanwhile, the double-layer encapsulation showed good adhesive at the interfaces characterized by SEM and red ink tests. The double-layer encapsulation can be accomplished in 40 min that shows promising potential for further gradient content layer encapsulation and scale-up application.

2 Results and discussion

2.1 Zirconia/siloxane composite

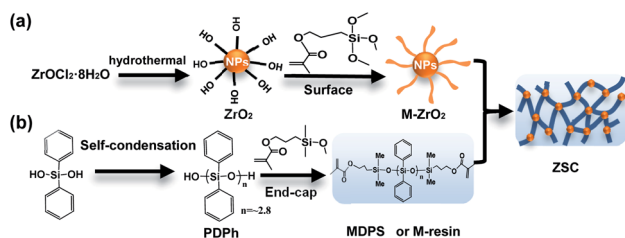Fig. 1 illustrates the preparation method for the transparent high RI ZSC. To achieve high RI of the ZSC, the matrix was designed as a high phenyl content siloxane. It was synthesized by methacryloxy end-capped of diphenylsiloxane oligomers (MDPS) (Fig. 2). The highly crystalline ZrO_2 nanoparticles were synthesized from a modified hydrothermal method at comparatively mild conditions.

The phenyl-siloxane products were monitored by FTIR and ^{29}Si-NMR (Fig. 2). In the FTIR spectrum (Fig. 2A), the strong absorption around 3070 cm^{-1}, 1728 cm^{-1}, and 1558 cm^{-1} are assigned to the =C–H, C=O, and C=C. After end-capped, the absorptions at 3290 cm^{-1} that assigned to Si–OH for poly-diphenylsiloxane oligomer are nearly disappeared.

In the ^{29}Si-NMR spectrum of the oligo-polydiphenylsiloxane, the peaks at *ca.* −46 ppm corresponds to the fully condensed Si (D^2) from $–O_2SiPh_2$, and the peaks at −40 ppm belongs to the Si (D^1) in –OSiPh–OH. After the end-cap reaction, the D^1 peak almost disappeared, and the peak corresponds to the Si (M^1) from $MASiMe_2O–$ appears at ∼10 ppm. From the corresponding peak area ratio, the polymerization degree of oligo-polydiphenylsiloxane (PDPh) is estimated as 2.8. After end-cap reaction, it is 4.1 (including end-capping groups), and the end-capping ratio is 96% (see ESI and Fig. S1†). The MDPS resin is highly transparent with an RI of 1.541 at 633 nm.

TEM and XRD analysis (Fig. 3, S2 and S3 in ESI†) show that the as-prepared ZrO_2 particles are highly crystalline tetragonal phases with an average size of ∼14 nm. The HR-TEM image in Fig. 3A shows that the spacing of the lattice fringe is about 0.252 nm that belongs to the tetragonal phase (110) crystal plane that agrees with the XRD result. Simulation from the XRD pattern of the modified nanoparticles (Fig. 3D) indicates that the ZrO_2 nanoparticles are tetragonal with a crystallinity of *ca.* 80% (Fig. S3†).

In the FTIR spectrum of the as-prepared ZrO_2 nanoparticle, the broad peak at ∼3330 cm^{-1} is assigned to the Zr–OH stretching. After surface modification, the Zr–OH absorption decreased, and new peaks at 1025 cm^{-1} assigned to the Si–O–Zr appear (Fig. 3E). The appearance of absorptions at 3070 cm^{-1}, 1728 cm^{-1}, and 1558 cm^{-1} assigned to the =C–H, C=O, and C=C respectively indicating the successful graft of the methacryloxylsiloxyl. After surface modification, the average diameter of the collected M-ZrO_2 nanoparticle increased a little bit to 17 nm (Fig. S2 ESI†). The M-ZrO_2 nanoparticle can then be well dispersed in THF and MDPS resin (Fig. 3A–C).

Fig. 1 The illustration of the preparation of the ZSC. (a) The high crystalline ZrO_2 nanoparticles were prepared by hydrothermal method and surface modification of MPTMS. (b) The synthesis of UV-curable high phenyl content MDPS resin.
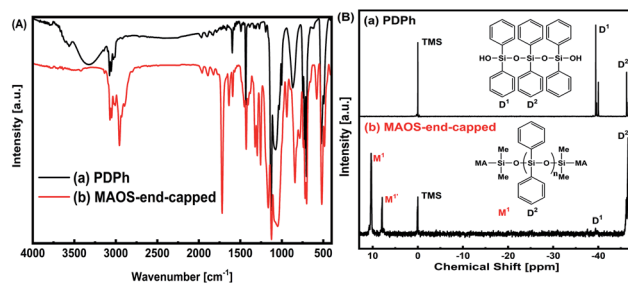

Fig. 2 The product of MDPS was characterized by (A) FT-IR spectra and (B) ^{29}Si-NMR spectra. In each digraph, spectra before (a) and after (b) MAOS end-cap are compared. MA represents methacryloyloxy.
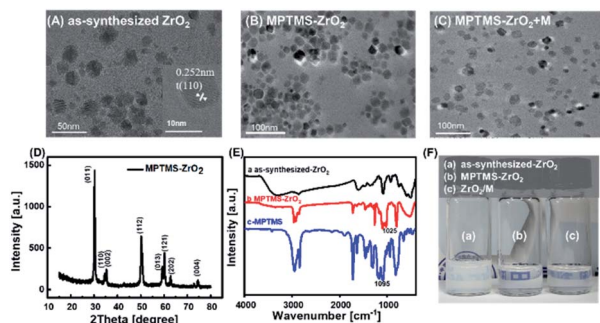
Fig. 3 (A–C) TEM images of (A) the as-synthesized ZrO_2 nanoparticles, the inset is an enlarged image of a single particle by HRTEM. (B) Zirconia nanoparticles after MPTMS modification (M-ZrO_2). (C) M-ZrO_2 nanoparticles dispersed in MDPS resin. (D) XRD pattern of the M-ZrO_2. (E) FT-IR spectra of (a) the as-synthesized ZrO_2 NPs, (b) M-ZrO_2 and (c) MPTMS. (F) Sample photos of (a) the as-synthesized ZrO_2 in THF, (b) M-ZrO_2 in THF and (c) M-ZrO_2/MDPS composite resin.

Transparent films were obtained from the ZSC with ZrO_2 content of 5–20 wt% (Fig. 4A). Although the transmittance decreases with the content of the ZrO_2 nano-particle, it is still 92.2% at 450 nm for the 20 wt% ZrO_2 content film. The RI of pure MDPS (M) resin, M-5, M-10, M-15, and M-20 at 633 nm was 1.540, 1.551, 1.573, 1.584, and 1.611, respectively, measured by Abbe refractometer (Fig. 4B). It has to be mentioned that when the RI of ZSC films were measured by ellipsometric method, the values were much higher. It probably because of the gradient distribution of ZrO_2 in the film, which need to be studied in detail in the future (Fig. S4†). Table 1 lists the optical and thermal properties of ZSCs with different ZrO_2 content (also see Fig. S5†). The RIs measured with different ZrO_2 content were generally agree with those calculated by Lorentz–Lorenz equation. The thermal stability of the nano-composites increases with the content of ZrO_2 wt% in term of both starting degradation temperature and residue at 800 °C.

2.2 LED encapsulation

It has been reported that for a single-layer encapsulant of LED (GaN) there is a maximum transmission coefficient of 0.8931 when the RI of the encapsulant reaches 1.612 (at 633 nm) according to Fresnel loss theory.[36,54] Once the RI exceeds the maximum value, the transmission coefficient begins to decline. When applying this theory to the above ZSC with ZrO_2 content
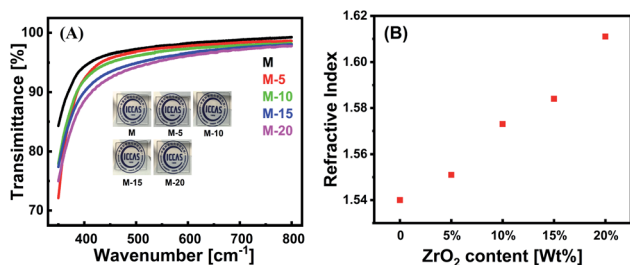

Fig. 4 (A) The optical transmittance curves of the composite films (~80 μm) with different ZrO_2 content; photos of the corresponding films on a glass substrate. (B) The measured values of ZSC film refractive index with different ZrO_2 content.

from 0 to 20%, the best transmittance is expected from the sample M-5 (RI = 1.551 at 633 nm), and the highest LEE is also expected. However, the experiments show that the transmittance obtained monotonically decreases with the ZrO_2 nanoparticle content from M to M-20 (Fig. 5A), and the LEE of the single-layer encapsulated was also monotonically decreased with ZrO_2 content (Fig. 5B).

In the above Fresnel loss simulation, it was assumed that only the RIs affect the result. For silicone nano-composites, the situation is more complicated, and the experimental data suggest that the light loss from nanoparticle scattering and the film thickness cannot be ignored even within nano-size below 20 nm. Fig. 5A shows that when the film thickness of ZSC increased from 80 μm to 280 μm, the transmittance of M-10 decreased from 94% to 85%, and the transmittance decreases more quickly when ZrO_2 content goes up (also seeing Fig. S5B ESI†).

If a double-layered encapsulant of MDPS (up layer) and ZSC (bottom layer) combination is used, it not only is more effective in decreasing the mismatch of RI between the substrate and air but also reduces the thickness of the composite film compare to single-layer encapsulation strategy that can greatly reduce the light scattering loss according to Rayleigh scattering theory. The effect of double-layer encapsulation can be estimated by the Fresnel transmission coefficient (FTC) expressed as eqn (1) and (2) that proposed by Mont *et al.*[54]

Fresnel loss:

$$R_{air} = \left(\frac{n_{air} - n_2}{n_{air} + n_2}\right)^2$$
$$R_1 = \left(\frac{n_1 - n_{chip}}{n_1 + n_{chip}}\right)^2 \quad (1)$$
$$R_2 = \left(\frac{n_2 - n_1}{n_2 + n_1}\right)^2$$

Fresnel transmission coefficient:

$$T_{air} = 1 - R_{air} = \left(\frac{4n_{air}n_2}{(n_{air} + n_2)^2}\right)$$
$$T_1 = 1 - R_1 = \frac{4n_1 n_{chip}}{(n_1 + n_{chip})^2}$$
$$T_2 = 1 - R_2 = \frac{4n_1 n_2}{(n_1 + n_2)^2} \quad (2)$$
$$T = T_{air} T_1 T_2 = \frac{64 n_1^2 n_2^2 n_{air} n_{chip}}{(n_1 + n_{chip})^2 (n_2 + n_1)^2 (n_{air} + n_2)^2}$$

where n_{chip} and n_{air} represent the RI values of the LED chip and air, taken as 2.60 and 1.0 at 633 nm, respectively. Where n_1 and n_2 represent the RI of the encapsulated material.

The simulation for double-layer encapsulation demonstrates that with the continuous change of refractive index combination (n_1 and n_2), the FTC results fall on a curved surface (Fig. 6A). The highest FTC of 0.9288 can be achieved when n_1 equals 1.89 and n_2 equals 1.37. When applied for the ZSC/MDPS samples, the calculated FTC values of double-layer encapsulation are all

Table 1 List of thermal and optical data of the ZSC with different zirconia content

Sample name	ZrO_2 [wt%]	ZrO_2 [v/v%]	T_d-10% [°C]	RI^a [633 nm]	RI^b [633 nm]	$T\%$ [633 nm]
M	0	0	315.2	1.54	—	98.5
M-5	5%	1.72%	317.7	1.55	1.55	98.0
M-10	10%	3.56%	330.2	1.57	1.56	97.5
M-15	15%	5.54%	340.6	1.58	1.57	96.6
M-20	20%	7.68%	353.7	1.61	1.58	96.5

^{a} Measured by Abbe refractometer at 633 nm. ^{b} Calculate from Lorentz–Lorenz equation: $\dfrac{n_c^2 - 1}{n_c^2 + 2} = \phi_p \dfrac{n_p^2 - 1}{n_p^2 + 2} + (1 - \phi_p) \dfrac{n_m^2 - 1}{n_m^2 + 2}$, where n_c is RI of ZSC; n_p is RI of ZrO_2; n_m is RI of MDPS resin.
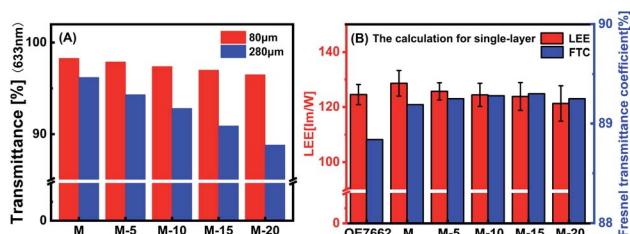

Fig. 5 (A) The transmittance of ZSC film (single layer) with different ZrO_2 content and thickness. (B) Red columns: LEE (light extraction efficiency) measured from LED encapsulated by a single layer of M, M-5, M-10, M-15, M-20, respectively; blue columns: the calculated FTC corresponding to the single-layer encapsulation.

higher than that of the single-layer encapsulation, and it increases with the ZrO_2 nanoparticle content in ZSC (Fig. 6B). The increase in FTC is more evident when the ZrO_2 content was from 0 to 10%.

The two-layer combination of ZSC (M-5, M-10, M-15, M-20) and MDPS (M) was also optimized by experimental characterization (Fig. 7). The thickness of the whole encapsulant is *ca.* 500 μm. A typical cross-section SEM photo of two-layer encapsulation is shown in Fig. S7.† It shows that all the double-layer encapsulation did lead to higher LEEs than those of single-layer
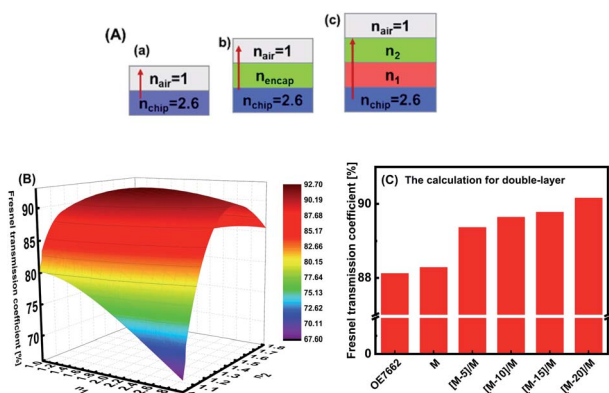

Fig. 6 (A) Schematic diagram of the refractive index combination and interfaces of (a) LED chip/air, (b) LED chip/singer layer encapsulant/air, and (c) LED chip/double-layer encapsulant/air. (B) The simulation of FTC is derived from eqn (2). (C) The calculated FTCs of doubled-layer encapsulation of M and ZSC/M with different ZrO_2 content.

encapsulation. The LEE increased obviously at the beginning when ZrO_2 nano-particle content increases from 0 to 10% in the ZSC layer, but then the LEE decreases with the ZrO_2 nano-particle content. The best LEE value was obtained from M-10/M (Fig. 7B) which is 11.2% higher than that of OE-7662 and 7.6% higher than that of M (MDPS single-layer encapsulation). The T_c of ZSC/M system encapsulated samples are in the range of 5000–6000 K, which is preferred for many commercial usages, while the T_c of OE-7662 is much higher in this case.

For LED, the water resistance and gas/vapor barrier property of the encapsulants are very important for the life time. In this work, it is demonstrated by the anti-sulfur vapor test and red ink test. The M-10/M double-layer encapsulated sample kept the highest LEE value after 2–4 hours of sulfur vapor corrosion. It is worth noticing that the novel polydiphenylsiloxane MDPS encapsulant has a much better anti-sulfur property itself, and
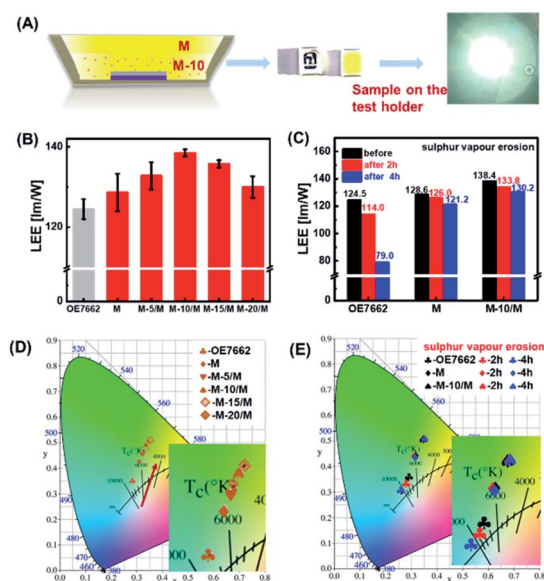

Fig. 7 (A) The schematic illustration of the double-layer encapsulated LED and photos of LED chip mounted on a substrate for testing. (B) The LEE data obtained from different combinations of double-layer encapsulation. (C) The comparison of LEE change with sulfur vapor erosion time. (D) The T_c of ZSC/M encapsulated samples with different ZrO_2 content. (E) The T_c before and after sulfur vapor erosion (OE-7662, M/M, M-10/M).

the composition of the ZrO$_2$ nanoparticle make the LEE value even higher. The LEE of OE-7662 was reduced by 8.4% and 36.5% respectively after 2 hours and 4 hours sulfur vapor corrosion, while the reduction of LEE of M-10/M double-layer encapsulated sample is 3.3% and 5.9% respectively upon 2 hours and 4 hours test (Fig. 7C). It means after 4 hours of sulfur vapor erosion, the LEE of M-10/M is 64.8% higher than that of the OE-7662. The T_c changes of M-10/M and M encapsulation kept within 1%, while that of OE-7662 drifted up by 40% (Fig. 7D and E).

All the double-layer encapsulated samples passed the red ink test showing that they have good adhesion with the chip substrate and anti-humidity property. There is no trace of red ink permeation and cracks can be observed by optical and SEM observation (Fig. S6 and S7†).

The SEM observation (Fig. 8A) also shows that the ZSC layer and the MDPS layer are well compatible and bonded. Fig. 8B shows that the SEM observation of the encapsulation of LED chip (M-10/M) after the red ink test. After the red ink test, the encapsulation resin has good adhesion to the substrate, and this also provides a basis for its anti-sulfur and stable LEE output.

3 Experimental section

3.1 Materials

Zirconyl chloride octahydrate (ZrOCl$_2$·8H$_2$O) was purchased from Aladdin. 2-Hydroxy-2-methylpropiophenone (97%) (photoinitiator-1173, 98%) was purchased from Sigma-Aldrich LLC. The phosphor YGG-530 was from China Minmetals Corporation. Irganox-1076 (>98%) and Irgafos-168 (>98%) were purchased from TCI. Trimethylolpropane trimethacrylate was purchased from Energy Chemical. Diphenylsilanediol (DPSD) (98%), 3-methacryloxypropyl-trimethoxysilane (MPTMS), and methacryloyloxydimethylmethoxysilane (MAOS) were purchased from Innochem (Beijing) Technology Co., Ltd. The reference silicone encapsulants OE-7662 were purchased from Dow Corning. Triethanolamine (TEA), tetrahydrofuran (THF) and toluene were purchase from Aladdin. All chemicals were used without further purification.

3.2 Synthesis and preparation

Preparation and modification of ZrO$_2$ nanoparticles. The highly crystalline tetragonal ZrO$_2$ nanoparticle was synthesized from a modified hydrothermal method.[1,50–52] Typically, 3.2 g (0.01 mol) of ZrOCl$_2$·8H$_2$O was dissolved in 95 ml of deionized water at room temperature under vigorous stirring. 4.5 g (0.03 mol) of TEA was added. Then an aqueous solution of about 4 M of NaOH was added until the solution pH value was about 9–10. Subsequently, the as-obtained zirconium hydroxide precursor was transferred into a Teflon-lined stainless steel autoclave with mechanic stirring. The solution was heated to 140–160 °C and kept for 4 h under the pressure of 0.5 MPa. During the reaction, the stirring speed was 600–1000 rpm. After cooling, a milky nanoparticle dispersion was obtained. The dispersion was centrifuged and repeatedly washed with DI water until neutral. The slurry of the ZrO$_2$ is collected and used for further modification. The yield was 41.3% which was obtained by drying part of the slurry in an oven at 80 °C for 12 hours.

For surface modification, ZrO$_2$, MPTMS with the mass ratio of 1 : 1.9 was mixed with 30 ml of THF. The mixture was first treated by ultrasound for 30 min and then stirred at 60 °C for 12 h. The product was precipitated by n-hexane and washed with ethanol to remove extra MPTMS and other residuals. The precipitation of MPTMS-ZrO$_2$ nanoparticles (M-ZrO$_2$) was re-dispersed in THF under ultrasonic.[1] The ZrO$_2$ content in M-ZrO$_2$ was estimated to be ~88 wt% by compare the RI of composite resin with ~5.7 wt% M-ZrO$_2$ (M-5 in Table 1) with that calculated from Lorentz–Lorenz equation.

Synthesis of the methacryl-diphenyl-polysiloxanes (MDPS). The MDPS was synthesized from non-catalyst condensation of DPSD and was then end-capped by MAOS.[19,21,52,53] A typical process is as follow. 1 mol DPSD in a round-bottomed flask was gradually heated up to 150 °C and vacuumed for 2 h. The temperature was then cooled down to 75 °C and a viscous liquid was obtained which was polydiphenylsiloxane (PDPh). 10 ml of toluene containing 1.5 mol MAOS and a trace of concentrated sulfuric acid was added under stirring. The mixture was then refluxed for another 2 h. The solution was washed with DI water until neutral. A transparent resin was obtained after removing the solvent and extra MAOS.

ZSC preparation and LED encapsulation. To prepare ZSC resin with 5 wt%, 10 wt%, 15 wt%, 20 wt% ZrO$_2$ content, typically, to 0.2 g of MDPS, 12 ml, 26 ml, 42 ml and 60 ml of M-ZrO$_2$ solution (1 mg/1 ml in THF) was added respectively. After removing the solvent by rotatory evaporator, the composite resin was then mixed with 10 wt% of phosphors, 0.4 wt% of Irganox-1076, 0.1 wt% of Irgafos-168, and 1 wt% of initiator-1173.[21] Finally 1 wt% of trimethylolpropane trimethacrylate was added. The mixture was then applied on the dry lensless-5050 lead-frame through a microsyringe. The amount of the encapsulant was carefully monitored so that each finished sample has an identical near the flat surface. The single-layer encapsulant was cured under 20 W LED UV light (365–405 nm) 30 min. For double-layer encapsulant, the second layer was applied after 10 min curing of the first layer, and it was cured for 30 min. Dow Corning OE-7662 with 10 wt% phosphors was applied for comparison which was cured at 80 °C for 1 h and 150 °C for 2 h.

3.3 Characterization

Fourier transform infrared spectrometry (FTIR) spectra were recorded by a Bruker EQUINOX55 spectrophotometer. [29]Si-
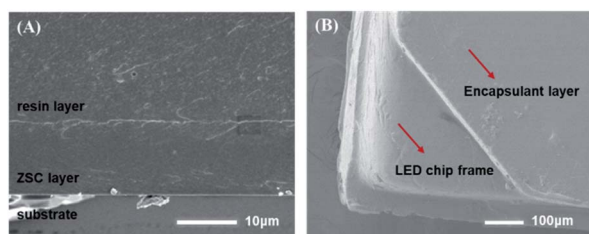

Fig. 8 (A) The SEM observation of the cross section of the two-layer film on silicon wafer (M-10/M). (B) The SEM observation of the encapsulation of LED chip (M-10/M) after the red ink test.

NMR spectrum was performed on Bruker 300 MHz instruments (DMX300) in THF solution with TMS and relaxation reagent (chromium acetylacetonate). X-ray diffraction (XRD) analysis was recorded on Empyrean. The transmission electron microscope (TEM) images were captured by TEM, JEM-2200FS, JEOL, Japan. The thermal gravimetric analysis (TGA) was performed on a PerkinElmer/Pyris 1 TGA by the heating rate of $20\,°C\,min^{-1}$ in a nitrogen atmosphere. The optical transmittance was measured by an ultraviolet-visible spectrophotometer (UV2600, SHIMADZU). RI of the L-MPS resin was measured by an Abbe refractometer (2WAJ, Shanghai Optical Instrument Factory No. 1). The LEE was detected by spectrophotocolorimeter with the LED spec analysis system (STC 4000, Everfine Photo-E-Info Co., Ltd.). The gas barrier property was demonstrated by the LEE and T_c change in the anti-sulfur test, in which samples and 1.34 g sulfur powder were kept at 105 °C for 4 h in an 800 ml sealed container. The red ink test was processed as follows. The 2% of red ink solution 2 ml was added to 100 ml DI water then heated to 100 °C. Then put the encapsulated LED chip into the solution and continued heating for 2 h. When the chip was cooled down to room temperature and dried in the air, it was observed under a microscope to find whether leakage happed, and the sample was also tested for the ability to be lit.

4 Conclusions

Transparent UV curable nano-composite ZSC with high RI was prepared from a highly crystalline ~14 nm ZrO_2 nano-particle and a polydiphenylsiloxane MDPS. When the ZrO_2 nano-particle content was increases from 0 to 20%, the RI of the composite increase from 1.54–1.61, and the transmittance was all above 92% with a film thickness of ~80 μm. The double-layer encapsulation M-10/M obtained 11.2% higher LEE compares to that of OE-7662, and higher LEE than those of the single-layer encapsulated samples. Furthermore, after 4 h of sulfur vapor erosion, the LEE of the M-10/M sample is 64.8% higher than that of OE-7662. At the same time, the T_c changes of M-10/M and M encapsulation kept within 1%, while that of OE-7662 drifted by 40%. The UV curing of the double layer encapsulation can be accomplished in 40 min which is still much time and energy saving compare to traditional thermal curing. The combination of highly crystalline zirconia nano-particles and UV curable polydiphenylsiloxane shows promising potential for further multi-layer LED encapsulation with enhanced quality.

Author contributions

The manuscript was written through the contributions of all authors. All authors have approved the final version of the manuscript.

Conflicts of interest

There are no conflicts to declare.

Acknowledgements

References

1 P.-T. Chung, S.-H. Chiou, C.-Y. Tseng and A. S. T. Chiang, *ACS Appl. Mater. Interfaces*, 2016, **8**(15), 9986–9993.

2 Y. H. Kim, J.-Y. Bae, J. Jin and B.-S. Bae, *ACS Appl. Mater. Interfaces*, 2014, **6**(5), 3115–3121.

3 H. J. Duan, W. J. Dong, X. Wang, X. X. Tao and H. R. Ma, *J. Appl. Polym. Sci.*, 2019, **136**(43), 9.

4 P.-H. Carlos, L. J. Guo and P.-F. Fu, *ACS Nano*, 2010, **4**(8), 4776–4784.

5 T. T. Zhao, R. Yu, S. Li, X. P. Li, Y. Zhang, X. Yang, X. J. Zhao, C. Wang, Z. C. Liu, R. Dou and W. Huang, *ACS Appl. Mater. Interfaces*, 2019, **11**(15), 14391–14398.

6 J.-Y. Bae, Y. H. Kim, H. Y. Kim, Y. B. Kim, J. h. Jin and B.-S. Bae, *ACS Appl. Mater. Interfaces*, 2015, **7**(2), 1035–1039.

7 M. Velderrain, Designing low permeability, optical-grade silicone systems: guidelines for choosing a silicone based on transmission rates for barrier applications, in *Advances in Display Technologies II*, International Society for Optics and Photonics, 2012.

8 S. Lee, J.-Y. Hong and J. Jang, *ACS Nano*, 2013, **7**(7), 5784–5790.

9 Y. Tokudome, T. Hara, R. Abe and M. Takahashi, *ACS Appl. Mater. Interfaces*, 2014, **6**(21), 19355–19359.

10 C. Zhang, C. Zhang, R. M. Ding, X. M. Cui, J. Wang, Q. H. Zhang and Y. Xu, *ACS Appl. Mater. Interfaces*, 2016, **8**(23), 14766–14775.

11 J. Gao, F. Bao, Q. X. Wu, R. Ma, X. B. Han, D. P. Jin, K. Y. Chena, J. Y. He, Z. F. Guo and C. J. Yan, *Mater. Today Commun.*, 2016, **7**, 149–154.

12 Y. H. Kim, Y.-W. Lim, D. Lee, Y. H. Kim and B.-S. Bae, *J. Mater. Chem. C*, 2016, **4**(46), 10791–10796.

13 J. Jin, S. Yang and B.-S. Bae, *J. Sol-Gel Sci. Technol.*, 2012, **61**(2), 321–327.

14 M. Zhao, Y. K. Feng, Y. Li, G. Li, Y. Wang, Y. Han, X. J. Sun and X. H. Tan, *J. Macromol. Sci., Part A: Pure Appl. Chem.*, 2014, **51**(8), 653–658.

15 J.-S. Kim, S. C. Yang, S.-Y. Kwak, Y. W. Choi, K.-W. Paik and B.-S. Bae, *J. Mater. Chem.*, 2012, **22**(16), 7954–7960.

16 T. C. Loh, C. M. Ng, R. N. Kumar, H. Ismail and Z. Ahmad, *J. Appl. Polym. Sci.*, 2017, **134**(37), 45285.

17 J.-Y. Bae, Y. H. Kim, H.-Y. Kim, Y.-W. Lim and B. S. Bae, *RSC Adv.*, 2013, **3**(23), 8871–8877.

18 J.-S. Kim, S. C. Yang and B.-S. Bae, *Chem. Mater.*, 2010, **22**(11), 3549–3555.

19 Y. H. Kim, Y.-W. Lim, D. Lee, Y. H. Kima and B.-S. Bae, *J. Mater. Chem. C*, 2016, **4**(46), 10791–10796.

20 S. C. Yang, S.-Y. Kwak, J. H. Jin, J.-S. Kim, Y. W. Choi, K.-W. Paik and B.-S. Bae, *J. Mater. Chem.*, 2012, **22**(18), 8874–8880.

21 X. X. Shang, S. Duan, M. Zhang, X. Y. Cao, K. Zheng, J. N. Zhang, Y. M. Ma and R. B. Zhang, *RSC Adv.*, 2018, **8**(17), 9049–9056.

22 P. Huang, H.-Q. Shi, H.-M. Xiao, Y.-Q. Li, N. Hu and S.-Y. Fu, *Sci. Rep.*, 2017, **7**(1), 5951.

23 C.-L. Tsai and G.-S. Liou, *Chem. Commun.*, 2015, **51**(70), 13523–13526.

24 T. Z. Guo, X. D. Lin, X. S. Hu, S. W. Cui and X. L. Chen, *Int. J. Polym. Anal. Charact.*, 2018, **23**(2), 120–127.

25 J.-Y. Bae, S. C. Yang, J. H. Jin, J.-S. Kim and B.-S. Bae, *J. Sol-Gel Sci. Technol.*, 2011, **58**(1), 114–120.

26 M. Ochi, D. Nii, Y. Suzuki and M. Harada, *J. Mater. Sci.*, 2010, **45**(10), 2655–2661.

27 Q. Lu and M. E. Mullins, *MRS Online Proc. Libr.*, 2012, **1400**, 23–28.

28 C.-C. Chang, L.-P. Cheng, F.-H. Huang, C.-Y. Lin, C.-F. Hsieh and W.-H. Wang, *J. Sol-Gel Sci. Technol.*, 2010, **55**(2), 199–206.

29 A. R. M. Dalod, O. G. Grendal, A. B. Blichfeld, V. Furtula, J. Pérez, L. Henriksen, T. Grande and M. Einarsrud, *Nanomaterials*, 2017, **7**(12), 460.

30 X. Zhao, L. Li, Z. Li and C. P. Wong, Stretchable and transparent silicone/zinc oxide nanocomposite for advanced LED packaging, in *2014 IEEE 64th Electronic Components and Technology Conference (ECTC)*, IEEE, 2014.

31 T. Otsuka and Y. Chujo, *Polym. J.*, 2008, **40**(12), 1157.

32 Y. W. Lai, L. J. Jin, J. Z. Hang, X. Y. Sun and L. Y. Shi, *J. Coat. Technol. Res.*, 2015, **12**(6), 1185–1192.

33 Y. Li, L. Wang, B. Natarajan, P. Tao, B. C. Benicewicz, C. Ullala and L. S. Schadler, *RSC Adv.*, 2015, **5**(19), 14788–14795.

34 K. Xu, S. Zhou and L. Wu, *Prog. Org. Coat.*, 2010, **67**(3), 302–310.

35 C. Liu, T. Hajagos, D. Y. Chen, Y. Chen, D. Kishpaugh and Q. B. Pei, *ACS Appl. Mater. Interfaces*, 2016, **8**(7), 4795–4802.

36 Y.-T. Lin, Y.-H. Li, I.-A. Lei, C.-Y. Kuo, C.-F. Lee, W.-Y. Chiu and T.-M. Don, *Mater. Chem. Phys.*, 2018, **206**, 136–143.

37 X. L. He, Z. Wang, Y. Pu, D. Wang, R. J. Tang, S. Cui, J.-X. Wang and J.-F. Chen, *Chem. Eng. Sci.*, 2019, **195**, 1–10.

38 Y. Li, P. Tao, R. W. Siegel and L. S. Schadler, *MRS Online Proc. Libr.*, 2013, **1547**, 161–166.

39 T. A. Cheema and G. Garnweitner, *CrystEngComm*, 2014, **16**(16), 3366–3375.

40 J. M. Park, H. S. Lee and H. M. Lim, Preparation and Characterization of Nano-size ZrO_2 Particle for Highly Refractive Index Nanocomposite Depending on Zirconium Precursor and Concentration, in *Materials Science Forum*, Trans Tech Publ., 2018.

41 P. T. Chung, C. T. Yang, S. H. Wang, C. W. Chen, A. S. T. Chiang and C.-Y. Liu, *Mater. Chem. Phys.*, 2012, **136**(2–3), 868–876.

42 P. Tao, Y. Li, R. W. Siegel and L. S. Schadler, *J. Appl. Polym. Sci.*, 2013, **130**(5), 3785–3793.

43 X. l. He, R. J. Tang, Y. Pu, J.-X. Wang, Z. Wang, D. Wang and J.-F. Chen, *Nano Energy*, 2019, **62**, 1–10.

44 W.-H. Liao, S.-T. Hsiao, Y.-F. Wu, S.-J. Zeng, S.-M. Li, Y.-S. Wang and C.-C. M. Ma, *RSC Adv.*, 2014, **4**(73), 38614–38622.

45 Y. Liu, Z. Y. Lin, X. Y. Zhao, C.-C. Tuan, K.-S. Moon, S. Yoo, M.-G. Jang and C.-P. Wong, *IEEE Trans. Compon., Packag., Manuf. Technol.*, 2014, **4**(7), 1125–1130.

46 J.-H. Huang, C.-P. Li, C.-W. C. Jian, K.-C. Lee and J.-H. Huang, *J. Taiwan Inst. Chem. Eng.*, 2015, **46**, 168–175.

47 N. Nakayama and T. Hayashi, *J. Appl. Polym. Sci.*, 2007, **105**(6), 3662–3672.

48 Y. Shen, L. Wang, H. Zhang, T. Wu and H. Y. Pan, *Materials Science and Engineering*, IOP Publishing, 2015.

49 X. L. He, Y. Pu, J.-X. Wang, D. Wang and J.-F. Chen, *Langmuir*, 2021, **37**(8), 2707–2713.

50 Y. Xia, C. Zhang, J.-X. Wang, D. Wang, X.-F. Zeng and J.-F. Chen, *Langmuir*, 2018, **34**(23), 6806–6813.

51 C.-W. Chen, X.-S. Yang and A. S. Chiang, *J. Taiwan Inst. Chem. Eng.*, 2009, **40**(3), 296–301.

52 X. Y. Cao, Y. Lu, X. P. Fan, Y. M. Ma, C. X. Yang, Z. H. Zhao, J. N. Zhang, K. Zheng, G. Ye, R. B. Zhang and S. B. Fang, CN2019111045869, 2019.

53 X. Y. Cao, X. P. Fan, Y. Lu, Y. M. Ma, C. X. Yang, Z. H. Zhao, J. N. Zhang, K. Zheng, G. Ye, R. B. Zhang, S. B. Fang and X. P. Fan, CN2019110991817, 2019.

54 F. W. Mont, J. K. Kim, M. F. Schubert, H. Luo, E. F. Schubert and R. W. Siegel, *High refractive index nanoparticle-loaded encapsulants for light-emitting diodes, Proc. SPIE 6486, Light-Emitting Diodes: Research, Manufacturing, and Applications XI*, Integrated Optoelectronic Devices, San Jose, CA, 2007.